# Strain-gradient elasticity and gradient-dependent plasticity with hierarchical refinement of NURBS

Isa Kolo, Lin Chen, René de Borst

*University of Sheffield, Department of Civil and Structural Engineering, Mappin Street, Sheffield S1 3JD, United Kingdom*

## Abstract

Higher-order strain-gradient models are relevant for engineering materials which exhibit size-dependent behaviour as observed from experiments. Typically, this class of models incorporate a length scale - related to micromechanical material properties - to capture size effects, remove stress singularities, or regularise an ill-posed boundary value problem resulting from localisation of deformation. The higher-order continuity requirement on shape functions can be met using NURBS discretisation, as is considered herein. However, NURBS have a tensor-product nature which makes selective refinement cumbersome. To maintain accuracy and efficiency in analysis, a finer mesh may be required, to capture a localisation band, certain geometrical features, or in regions with high gradients. This work presents strain-gradient elasticity and strain-gradient plasticity, both of second-order, with hierarchically refined NURBS. Refinement is performed based on a multi-level mesh with element-wise hierarchical basis functions interacting through an inter-level subdivison operator. This ensures a standard finite-element data structure. Suitable marking strategies have been used to select elements for refinement. The capability of the numerical schemes is demonstrated with two-dimensional examples.

*Keywords:* Gradient elasticity, Gradient plasticity, Isogeometric analysis, NURBS, Hierarchical refinement, Adaptivity

## 1. Introduction

Isogeometric analysis has been proposed as a means to integrate engineering design and analysis [1]. Essentially, the spline-based basis functions

used in design - such as the widely-used Non-Uniform Rational B-splines (NURBS) - are used in analysis as well. This eliminates geometrical approximation errors in converting a geometry to a standard finite element mesh based on Lagrange polynomial functions. Furthermore, NURBS have a natural higher-order character. This has motivated their use in higher-order gradient models where higher-order continuity is needed [2, 3, 4, 5]. In these models, a length scale is incorporated in order to capture size effects and/or maintain a mesh-objective solution after the onset of softening.

Incorporating a length scale makes gradient elasticity models capable of removing stress singularities at crack tips [6]. In problems associated with softening such as gradient plasticity and damage, localisation of deformation can develop. To accurately capture localisation bands and geometrical singularities, and in areas with strong gradients, there is need for a finer mesh in certain regions of the geometry [7, 8]. However, NURBS have a tensor-product nature which makes this local refinement a non-trivial task. Truncated-Hierarchical B-Splines (THB) and NURBS have been developed to address this [9]. More recently, THB splines have been expressed in a convenient element-wise data structure via Beziér extraction, thereby eliminating the need for explicit truncation of bases [10, 11].

Several works have addressed adaptive refinement of generalized or gradient continua in the standard finite element context including the associated transfer of variables, e.g. [12, 13, 14, 15, 16]. In the context of hierarchical NURBS, Hennig et al. [17] explored various transfer operators and applied them to both linear and non-linear problems. However, adaptive refinement of gradient-plasticity using hierarchical NURBS still remains to be addressed. If strain-gradient continua are to be widely adopted for analyses, the use of adaptive refinement techniques is a *conditio sine qua non*. Herein, strain-gradient models, gradient elasticity and gradient plasticity specifically, are explored using adaptive meshing techniques to efficiently capture failure and/or geometrical singularities.

We start by giving an overview of the gradient formulations considered herein - Aifantis' gradient elasticity formulation [18, 19] and the implicit gradient plasticity formulation [20]. The weak forms and discretisation in the isogeometric analysis context are outlined next. The next section highlights hierarchical basis functons and their implementation via inter-level subdivision operators. Section 5 discusses the adaptive hierarchical refinement procedure including element marking and the transfer of variables between levels. We proceed with a section on numerical examples. First, for gradient

2

elasticity and classical plasticity, for which exact solutions exist, and then gradient plasticity. The energy norm of the error is used in the former case, while a largely heuristic marking strategy is used for the latter. A concluding section ends the paper.

## 2. Strain-gradient formulations

### 2.1. Aifantis' gradient elasticity

The gradient elasticity theory of Aifantis [18, 19] is considered here. In this theory, the Laplacian of the strain is introduced into the classical linear elastic constitutive relations as follows:

$$\boldsymbol{\sigma} = \mathbf{D}^e(\boldsymbol{\varepsilon} - \ell^2 \nabla^2 \boldsymbol{\varepsilon}) \tag{1}$$

where $\boldsymbol{\sigma} = [\sigma_{xx}, \sigma_{yy}, \sigma_{zz}, \sigma_{xy}, \sigma_{yz}, \sigma_{zx}]^{\mathrm{T}}$ is the stress vector, $\ell$ is a length scale parameter, $\boldsymbol{\varepsilon} = [\varepsilon_{xx}, \varepsilon_{yy}, \varepsilon_{zz}, \tau_{xy}, \tau_{yz}, \tau_{zx}]^{\mathrm{T}}$ is the strain vector, and $\mathbf{D}^e$ is the material elastic stiffness matrix given by

$$\mathbf{D}^e = \begin{bmatrix} \lambda + 2\mu & \lambda & \lambda & 0 & 0 & 0 \\ \lambda & \lambda + 2\mu & \lambda & 0 & 0 & 0 \\ \lambda & \lambda & \lambda + 2\mu & 0 & 0 & 0 \\ 0 & 0 & 0 & \mu & 0 & 0 \\ 0 & 0 & 0 & 0 & \mu & 0 \\ 0 & 0 & 0 & 0 & 0 & \mu \end{bmatrix}. \tag{2}$$

for an isotropic linear elastic material where $\lambda$ and $\mu$ are the Lamé constants. The accompanying equilibrium equations are:

$$\mathbf{L}^T \boldsymbol{\sigma} = \mathbf{0} \tag{3}$$

where body forces have been neglected and $\mathbf{L}$ is the differential operator:

$$\mathbf{L} = \begin{bmatrix} \frac{\partial}{\partial x} & 0 & 0 & \frac{\partial}{\partial y} & \frac{\partial}{\partial z} & 0 \\ 0 & \frac{\partial}{\partial y} & 0 & \frac{\partial}{\partial x} & 0 & \frac{\partial}{\partial z} \\ 0 & 0 & \frac{\partial}{\partial z} & 0 & \frac{\partial}{\partial x} & \frac{\partial}{\partial y} \end{bmatrix}^{\mathrm{T}}. \tag{4}$$

Substituting the stress-strain relation, eq.(1), and assuming small displacement gradients,

$$\boldsymbol{\varepsilon} = \mathbf{L}\mathbf{u}, \tag{5}$$

3

the following fourth-order partial differential equation results:

$$\mathbf{L}^T \mathbf{D}^e \mathbf{L}(\mathbf{u} - \ell^2 \nabla^2 \mathbf{u}) = \mathbf{0} \tag{6}$$

where $\mathbf{u} = [u_x, u_y, u_z]^T$ is the displacement vector and $\nabla^2 \equiv \nabla^T \cdot \nabla$ is the Laplacian operator with $\nabla = [\frac{\partial}{\partial x}, \frac{\partial}{\partial y}, \frac{\partial}{\partial z}]^T$.

## 2.2. Implicit gradient plasticity

We adopt the implicit gradient plasticity formulation [20]. As in the previous section, limiting our scope to small deformations with no body forces, the problem is defined by the equilibrium equation:

$$\mathbf{L}^T \boldsymbol{\sigma} = \mathbf{0} \tag{7}$$

the kinematic relation

$$\boldsymbol{\varepsilon} = \mathbf{L}\mathbf{u} \tag{8}$$

and the following incremental constitutive equations

$$\mathrm{d}\boldsymbol{\sigma} = \mathbf{D}^e(\mathrm{d}\boldsymbol{\varepsilon} - \mathrm{d}\boldsymbol{\varepsilon}^p) \tag{9}$$

$$\mathrm{d}\boldsymbol{\varepsilon}^p = \mathrm{d}\lambda \mathbf{m}, \quad \mathbf{m} = \frac{\partial F}{\partial \boldsymbol{\sigma}} \tag{10}$$

where an associated plasticity flow rule has been adopted for the yield function $F$. In equations (7)-(10), $\boldsymbol{\sigma}$, $\boldsymbol{\varepsilon}$, $\mathbf{u}$, $\mathbf{D}^e$ and $\mathbf{L}$ are as defined for gradient elasticity, $\mathrm{d}\boldsymbol{\varepsilon}^p$ is the plastic strain increment vector, $\mathrm{d}\lambda$ is a non-negative plastic multiplier, and $\mathbf{m}$ is a vector that defines the direction of plastic flow relative to $F$. The yield function $F$ is given by [20]:

$$F(\boldsymbol{\sigma}, \kappa, \bar{\kappa}) = \sigma_e(\boldsymbol{\sigma}) - (1 - \omega(\bar{\kappa}))\,\sigma_y(\kappa) \tag{11}$$

$$\sigma_y = \sigma_{y,0} + H\kappa \tag{12}$$

$$\omega(\bar{\kappa}) = 1 - e^{-\beta\bar{\kappa}} \tag{13}$$

$$\mathrm{d}\kappa = \mathrm{d}\lambda \tag{14}$$

subject to the constraints

$$\mathrm{d}\lambda \geq 0, \quad F \leq 0, \quad F\mathrm{d}\lambda = 0 \tag{15}$$

where $\sigma_e(\boldsymbol{\sigma})$ is the Von Mises equivalent stress, $\kappa$ is the local effective plastic strain measure or hardening parameter, $\bar{\kappa}$ is the nonlocal effective plastic

4

strain measure, $\sigma_y$ is the yield or flow stress, $\sigma_{y,0}$ is the initial yield strength, $H > 0$ is the hardening modulus, $\omega \in [0, 1]$ is a nonlocal damage variable, and $\beta$ is a material constant. The strain-hardening hypothesis has been adopted to obtain a relation for the hardening parameter increment $\mathrm{d}\kappa$ in eq.(14).

The nonlocal effective plastic strain measure, $\bar{\kappa}(\mathbf{x})$, is defined as the volume average of the local effective plastic strain measure, $\kappa = \kappa(\boldsymbol{\varepsilon}^p)$. The ensuing formulation can be approximated as [20]:

$$\bar{\kappa}(\mathbf{x}) - \ell^2 \nabla^2 \bar{\kappa}(\mathbf{x}) = \kappa(\mathbf{x}) \tag{16}$$

where $\ell$ is the length scale that sets the averaging volume. The length scale, which can be correlated with micro-properties of a material, sets requirements on the mesh. In localisation problems, the mesh size needs to be at least three times smaller than $2\pi\ell$ for sufficient accuracy to be achieved [21, 22, 23].

The strain-hardening hypothesis is assumed to also hold for $\bar{\kappa}$. For a state variable $\bar{\lambda}$ defined as

$$\bar{\lambda}(t) = \max\{\bar{\kappa}(\tau)|0 \leq \tau \leq t\} \tag{17}$$

the following constraints apply:

$$\mathrm{d}\bar{\lambda} \geq 0, \quad \bar{\kappa} - \bar{\lambda} \leq 0, \quad \mathrm{d}\bar{\lambda}\left[\bar{\kappa} - \bar{\lambda}\right] = 0 \tag{18}$$

Standard static and kinematic boundary conditions are adopted on the body surface $S$:

$$\boldsymbol{\Upsilon}\mathbf{n}_s = \mathbf{t}, \quad \mathbf{u} = \mathbf{u}_s \tag{19}$$

where $\boldsymbol{\Upsilon}$ is the stress tensor in matrix form, $\mathbf{n}_s$ is the outward normal to the surface $S$, and $\mathbf{t}$ is the boundary traction vector. Natural boundary conditions are assumed to apply on the derivative of $\bar{\kappa}$ [24]:

$$(\mathbf{n}_s^{\mathrm{T}}\nabla)\bar{\kappa} = 0. \tag{20}$$

Eq.(16) has to be satisfied in addition to the equilibrium equation, and thus, two equations have to be discretised and solved at each load step.

To update the stress, the trial yield function is evaluated at every iteration $j + 1$ using [20]:

$$F_t = F(\boldsymbol{\sigma}_t, \kappa_0, \bar{\kappa}_{j+1}) = \sigma_{e,t} - \sigma_{y,0}\left(1 - \omega_{j+1}\right) \tag{21}$$

5

where $\sigma_{e,t} = \sigma_e(\boldsymbol{\sigma}_t)$ is the Von Mises equivalent stress evaluated with the trial stress, $\boldsymbol{\sigma}_t$ :

$$\boldsymbol{\sigma}_t = \boldsymbol{\sigma}_0 + \mathbf{D}^e \Delta \boldsymbol{\varepsilon}_{j+1}. \tag{22}$$

and $(\bullet)_0$ indicates value at previous converged load step. When $F_t \leq 0$, there is an elastic state and the stress is simply updated as $\boldsymbol{\sigma}_{j+1} = \boldsymbol{\sigma}_t$. When $F_t > 0$, the state is plastic and is updated using [25, 23]:

$$\boldsymbol{\sigma}_{j+1} = \boldsymbol{\sigma}_t - \Delta\gamma_{j+1} \mathbf{D}^e \mathbf{m}_t \tag{23}$$

where $\mathbf{m}_t$ is given by Equation $(10)_2$, and $\Delta\gamma_{j+1}$ is the amount of plastic strain for the current iteration, given by [20],

$$\Delta\gamma_{j+1} = \frac{F_t}{H\left[1 - \omega_{j+1}\right]\left[\frac{\partial \kappa}{\partial \lambda}\right] + \frac{3E}{2(1+\nu)}} \tag{24}$$

in which $E$ is the Young's modulus and $\nu$ is the Poisson ratio.

## 3. Isogeometric finite element discretisation

### 3.1. NURBS shape functions

The shape functions of a univariate NURBS are a generalisation of the B-spline shape functions:

$$R_{a,p}(\xi) = \frac{w_a B_{a,p}(\xi)}{\mathbf{W}(\xi)} \tag{25}$$

where $B_{a,p}$ is the B-spline shape function, $w_a$ is the corresponding weight and $\mathbf{W}$ is the weight function given by:

$$\mathbf{W}(\xi) = \sum_{b=1}^{n} w_b B_{b,p}(\xi) \tag{26}$$

For a parametric coordinate $\xi$ and a polynomial of degree $p = 0$, the B-spline shape function is defined as:

$$B_{a,0}(\xi) = \begin{cases} 1, & \xi_a \leq \xi \leq \xi_{a+1} \\ 0, & \text{otherwise} \end{cases} \tag{27}$$

and for $p > 0$, it is defined by the Cox–de Boor recursion formula [26, 27]:

$$B_{a,p}(\xi) = \frac{\xi - \xi_a}{\xi_{a+p} - \xi_a} B_{a,p-1}(\xi) + \frac{\xi_{a+p+1} - \xi}{\xi_{a+p+1} - \xi_{a+1}} B_{a+1,p-1}(\xi) \tag{28}$$

Tensor products of univariate NURBS shape functions are used to obtain multivariate shape functions.

## 3.2. Bézier element

The Bézier extraction operator, $\mathbf{C}$, is used to decompose a NURBS mesh into $\mathcal{C}^0$-continuous Bézier elements [28, 29]. This is done to enable a standard finite element analysis format with basis functions local to an element. For a two-dimensional element $e$, the NURBS basis functions are expressed as:

$$\mathbf{N}^e(\xi, \eta) = \mathbf{W}^e \mathbf{C}^e \frac{\mathbf{B}^e(\xi, \eta)}{W^e(\xi, \eta)} \tag{29}$$

with

$$W^e(\xi, \eta) = (\mathbf{w}^e)^T \mathbf{C}^e \mathbf{B}^e(\xi, \eta) \tag{30}$$

where $\eta$ is the parametric coordinate in the second spatial dimension, $\mathbf{N}$ is a matrix containing the NURBS shape functions, $\mathbf{w}$ is a vector of the NURBS weights, and $\mathbf{B}$ contains the Bézier shape functions.

## 3.3. Weak forms and spatial discretisation

### 3.3.1. Gradient elasticity

The equilibrium equation - eq.(6) - is premultiplied by a test function $\tilde{\mathbf{u}}$ and integrated over the domain $\mathbf{\Omega}$. It is further integrated by parts, and by employing the Green's theorem, the following weak form results:

$$\int_\Omega \tilde{\boldsymbol{\varepsilon}}^T \mathbf{D} \boldsymbol{\varepsilon} d\Omega + \sum_{i=1}^3 \int_\Omega \ell^2 \frac{\partial \tilde{\boldsymbol{\varepsilon}}^T}{\partial x_i} \mathbf{D} \frac{\partial \boldsymbol{\varepsilon}}{\partial x_i} d\Omega = $$
$$\int_\Omega \tilde{\mathbf{u}}^T \mathbf{b} d\Omega + \int_{\Gamma_n} \tilde{\mathbf{u}}^T \mathbf{t} d\Gamma + \sum_{i=1}^3 \oint_\Gamma \ell^2 (\mathbf{n} \cdot \nabla \tilde{\mathbf{u}})^T \mathbf{D} \frac{\partial \boldsymbol{\varepsilon}}{\partial x_i} d\Gamma \tag{31}$$

where $\mathbf{t}$ is the prescribed tractions on the Neumann part of the boundary $\Gamma_n$ and $\mathbf{n}$ is the normal vector to the boundary [30]. $\tilde{\boldsymbol{\varepsilon}}$ is the virtual strain, $\tilde{\boldsymbol{\varepsilon}} = \mathbf{L}\tilde{\mathbf{u}}$. When the derivatives of $\tilde{\boldsymbol{\varepsilon}}$ are assumed to vanish on the boundary, the last term also vanishes.

The displacements $\mathbf{u}$ are related to the discrete displacements $\mathbf{a} = [a_{1x}, a_{1y}, a_{1z}, a_{2x}, a_{2y}, a_{2z}, \ldots]^T$ in the control points via:

$$\mathbf{u} = \mathbf{N}_u \mathbf{a} \tag{32}$$

where $\mathbf{N}_u$ is the matrix which contains the NURBS shape functions:

$$\mathbf{N}_u = \begin{bmatrix} N_1 & 0 & 0 & N_2 & 0 & 0 & \cdots & N_{ns} & 0 & 0 \\ 0 & N_1 & 0 & 0 & N_2 & 0 & \cdots & 0 & N_{ns} & 0 \\ 0 & 0 & N_1 & 0 & 0 & N_2 & \cdots & 0 & 0 & N_{ns} \end{bmatrix} \tag{33}$$

and $ns$ is the number of shape functions at each control point. A relation similar to eq. (32) holds for the variations of the continuous and nodal displacements, $\delta\mathbf{u}$ and $\delta\mathbf{a}$. When the discretised variables are used, eq.(31) leads to

$$[\mathbf{K}_1 + \mathbf{K}_2]\mathbf{a} = \mathbf{f}^{ext} \tag{34}$$

with the standard stiffness matrix

$$\mathbf{K}_1 = \int_\Omega \mathbf{B}^T\mathbf{D}\mathbf{B}d\Omega, \tag{35}$$

the matrix containing higher-order derivatives

$$\mathbf{K}_2 = \sum_{i=1}^3 \int_\Omega \ell^2 \frac{\partial \boldsymbol{B}^T}{\partial x_i}\mathbf{D}\frac{\partial \boldsymbol{B}}{\partial x_i}d\Omega, \tag{36}$$

and the external force vector

$$\mathbf{f}^{ext} = \int_\Omega \mathbf{N_u}^T\mathbf{b}d\Omega + \int_{\Gamma_n} \mathbf{N_u}^T\mathbf{t}d\Gamma \tag{37}$$

in which $\mathbf{B} = \mathbf{L}\mathbf{N}_u$. Second partial derivatives have to be computed, and hence $\mathcal{C}^1$-continuous shape functions are required. Quadratic NURBS have been adopted here.

### 3.3.2. Gradient plasticity

As alluded to before, eq.(16) has to be solved in addition to the equilibrium equation. The former and latter are premultiplied with the variational quantities $\delta\mathbf{u}$ and $\delta\bar{\lambda}$, respectively, and set to zero. Using integration by parts, the divergence theorem, the kinematic equation - eq.(8), the incremental constitutive relation, eq.(9), and the following linearisations at iteration $j+1$ of the Newton-Raphson iterative scheme,

$$\boldsymbol{\sigma}_{j+1} = \boldsymbol{\sigma}_j + \mathrm{d}\boldsymbol{\sigma}; \quad \kappa_{j+1} = \kappa_j + \mathrm{d}\kappa; \quad \bar{\kappa}_{j+1} = \bar{\kappa}_j + \mathrm{d}\bar{\kappa}, \tag{38}$$

8

leads to the following weak forms for the equilibrium and nonlocal effective strain equations respectively [20, 31]:

$$\int_V \delta\boldsymbol{\varepsilon}^{\mathrm{T}}\mathbf{D}^e(\ \mathrm{d}\boldsymbol{\varepsilon} - \mathrm{d}\lambda\mathbf{m})dV = \int_S \delta\mathbf{u}^{\mathrm{T}}\mathbf{t}_{j+1}\mathrm{d}S - \int_V \delta\boldsymbol{\varepsilon}^{\mathrm{T}}\boldsymbol{\sigma}_j dV \qquad (39)$$

$$\int_V \left( \delta\bar{\lambda}\mathrm{d}\bar{\kappa} - \ell^2(\nabla\delta\bar{\lambda})^{\mathrm{T}}(\nabla\mathrm{d}\bar{\kappa}) - \delta\bar{\lambda}\mathrm{d}\kappa \right) dV =$$
$$- \int_V \left( \delta\bar{\lambda}\bar{\kappa}_j - \ell^2(\nabla\delta\bar{\lambda})^{\mathrm{T}}(\nabla\bar{\kappa}_j) - \delta\bar{\lambda}\kappa_j \right) dV \qquad (40)$$

The nonlocal effective plastic strain measure is discretised in addition to the displacement field thus

$$\bar{\lambda} = \mathbf{h}^{\mathrm{T}}\bar{\boldsymbol{\Lambda}} \qquad (41)$$

where the vector $\bar{\boldsymbol{\Lambda}}$ contains the nonlocal plastic multiplier degrees of freedom at the control point, and $\mathbf{h}$ is a vector containing NURBS shape functions. The same order of interpolation is used for the interpolation of the displacements and the nonlocal plastic multiplier, i.e. $\mathbf{N}_u$ and $\mathbf{h}$ both contain quadratic NURBS [31].

Next, the discretised variables are employed in the weak forms - eq.(39) and eq.(40). Requiring the result to hold for all admissible $\delta\mathbf{a}$ and $\delta\bar{\boldsymbol{\Lambda}}$ leads to the following set of incremental non-linear algebraic equations [20]:

$$\begin{bmatrix} \mathbf{K}_{aa} & \mathbf{K}_{a\lambda} \\ \mathbf{K}_{\lambda a} & \mathbf{K}_{\lambda\lambda} \end{bmatrix} \begin{bmatrix} \mathrm{d}\mathbf{a} \\ \mathrm{d}\bar{\boldsymbol{\Lambda}} \end{bmatrix} = \begin{bmatrix} \mathbf{f}_e - \mathbf{f}_a \\ -\mathbf{f}_\lambda \end{bmatrix} \qquad (42)$$

where the matrices are defined as

$$\mathbf{K}_{aa} = \int_V \mathbf{B}^{\mathrm{T}}\mathbf{A}_{aa}\mathbf{B}\mathrm{d}V, \qquad (43)$$

$$\mathbf{K}_{a\lambda} = -\int_V \mathbf{B}^{\mathrm{T}}\mathbf{A}_{a\lambda}\mathbf{h}\ \mathrm{d}V \qquad (44)$$

$$\mathbf{K}_{\lambda a} = -\int_V \mathbf{h}^{\mathrm{T}}\mathbf{A}_{\lambda a}\mathbf{B}\ \mathrm{d}V, \qquad (45)$$

$$\mathbf{K}_{\lambda\lambda} = \int_V \mathbf{h}^{\mathrm{T}}\big(1 - A_{\lambda\lambda}\big)\mathbf{h} + \ell^2(\nabla\bar{\lambda})^{\mathrm{T}}(\nabla\bar{\lambda})\ \mathrm{d}V, \qquad (46)$$

and the force vectors are expressed as

$$\mathbf{f}_e = \int_S \mathbf{N}^{\mathrm{T}}\mathbf{t}_{j+1}\mathrm{d}S, \qquad (47)$$

9

$$\mathbf{f}_a = -\int_V \mathbf{B}^\mathrm{T}\boldsymbol{\sigma}_j \mathrm{d}V, \tag{48}$$

$$\mathbf{f}_\lambda = \mathbf{K}_\lambda \bar{\lambda}_j - \int_V \mathbf{h}^\mathrm{T}\lambda_j \, \mathrm{d}V \tag{49}$$

where

$$\mathbf{K}_\lambda = \int_V \mathbf{h}^\mathrm{T}\mathbf{h} + \ell^2(\nabla\bar{\lambda})^\mathrm{T}(\nabla\bar{\lambda}) \, \mathrm{d}V. \tag{50}$$

The arrays $\mathbf{A}_{aa}$, $\mathbf{A}_{a\lambda}$ and $\mathbf{A}_{\lambda a}$, and the scalar $A_{\lambda\lambda}$ are defined as [20, 25]:

$$\mathbf{A}_{aa} = \mathbf{A} - \frac{\mathbf{A}\mathbf{m}\mathbf{m}^\mathrm{T}\mathbf{A}}{H\left(1-\omega\right)\left(\frac{\partial\kappa}{\partial\lambda}\right) + \frac{3E}{2(1+\nu)}} \tag{51}$$

$$\mathbf{A}_{a\lambda} = \frac{\sigma_y\left(\frac{\partial\omega}{\partial\bar{\kappa}}\right)\left(\frac{\partial\bar{\kappa}}{\partial\lambda}\right)\mathbf{A}\mathbf{m}}{H\left(1-\omega\right)\left(\frac{\partial\kappa}{\partial\lambda}\right) + \frac{3E}{2(1+\nu)}} \tag{52}$$

$$\mathbf{A}_{\lambda a} = \frac{\mathbf{m}^\mathrm{T}\mathbf{A}}{H\left(1-\omega\right)\left(\frac{\partial\kappa}{\partial\lambda}\right) + \frac{3E}{2(1+\nu)}} \tag{53}$$

$$A_{\lambda\lambda} = \frac{\sigma_y\left(\frac{\partial\omega}{\partial\bar{\kappa}}\right)\left(\frac{\partial\bar{\kappa}}{\partial\lambda}\right)}{H\left(1-\omega\right)\left(\frac{\partial\kappa}{\partial\lambda}\right) + \frac{3E}{2(1+\nu)}} \tag{54}$$

respectively, where $\mathbf{A}$ is the algorithmic stiffness operator

$$\mathbf{A} = \left[(\mathbf{D}^e)^{-1} + \Delta\gamma\frac{\partial\mathbf{m}}{\partial\boldsymbol{\sigma}}\right]^{-1} \tag{55}$$

## 4. Hierarchical refinement of NURBS

In hierarchical refinement, a multi-level mesh is used after determining the appropriate active elements across different hierarchical levels. Here, an element-wise approach conforming with the Beziér extraction framework is adopted.

### 4.1. Hierarchical bases

We consider a univariate B-spline in a parametric domain $\boldsymbol{\Omega}_d$ with knot vector $\boldsymbol{\Xi}$ and polynomial degree $p$. A hierarchy of $P$ levels is constructed by successive uniform knot insertions from an initial knot vector $\boldsymbol{\Xi}^0$ until $\boldsymbol{\Xi}^{P-1}$ within $\boldsymbol{\Omega}_d$. Hence, nested parametric domains $\boldsymbol{\Omega}_d^i \subset \boldsymbol{\Omega}_d^{i+1}$ and nested

10

knot vectors $\mathbf{\Xi}^i \subset \mathbf{\Xi}^{i+1}$ arise. The NURBS basis functions $\mathbf{N}^i = \left\{N_j^i\right\}_{j=1}^{n_i}$, defined by the knot vector of each level $\mathbf{\Xi}^i$ $(i = 0, 1, \ldots, P-1)$, form a nested approximation space $\mathcal{N}^i$. The basis function of each hierarchical level $i$ can be expressed as a linear combination of each higher level $j$ due to the nested nature of $\mathcal{N}^i$:

$$\mathbf{N}^i = \mathbf{S}^{i,j}\mathbf{N}^j = \prod_{l=i}^{j-1} \mathbf{S}^{L,L+1}\mathbf{N}^{L+1} \tag{56}$$

where $\mathbf{S}^{L,L+1}$ is the refinement or subdivision operator given by:

$$S_{IJ}^{L,L+1} = \frac{w_I^L}{w_J^{L+1}} M_{IJ}^{L,L+1} \tag{57}$$

in which $M_{IJ}^{L,L+1}$ is an entry in the linear subdivision operator for the B-spline shape functions between the hierarchical levels $L$ and $L + 1$. The B-spline shape functions of the hierarchical levels $L$ and $L + 1$ are defined by knot vectors $\mathbf{\Xi}^L$ and $\mathbf{\Xi}^{L+1}$ respectively, using a weight factor $w = 1$. $w_I^L$ represents the weight factor of the $I$th shape function on hierarchical level $L$.

The hierarchical basis function space $\mathcal{A}$ is defined as

$$\mathcal{A} = \bigcup_{L=0}^{P-1} \mathcal{A}_a^L \quad \text{with} \quad \mathcal{A}_a^L = \mathcal{A}^L \backslash \mathcal{A}_-^L \tag{58}$$

where "$\backslash$" is the logic NOT and $\mathcal{A}_a^L$ are the active basis functions of hierarchical level $L$. $\mathcal{A}^L$ is the union of basis functions defined over the active elements on hierarchical level $L$. $\mathcal{A}_-^L$ denotes the shape functions in $\mathcal{A}^L$ with support over the active elements on coarser hierarchical levels. Another shape function variable $\mathcal{A}_+^L$ denotes those with support over active elements on finer hierarchical levels. Succinctly, we have the following set of basis functions:

$$\mathcal{A}^L = \left\{N_j^L \in \mathcal{N}^L : \ \mathrm{sup}N_j^L \bigcap E_A^L \neq \emptyset\right\}$$

$$\mathcal{A}_+ = \bigcup_{L=0}^{P-1} \mathcal{A}_+^L \quad \text{with} \quad \mathcal{A}_+^L = \left\{N_j^L \in \mathcal{A}^L : \ \mathrm{sup}N_j^L \bigcap \mathbf{\Omega}_d^{L+} \neq \emptyset\right\} \tag{59}$$

$$\mathcal{A}_- = \bigcup_{L=0}^{P-1} \mathcal{A}_-^L \quad \text{with} \quad \mathcal{A}_-^L = \left\{N_j^L \in \mathcal{A}^L : \ \mathrm{sup}N_j^L \bigcap \mathbf{\Omega}_d^{L-} \neq \emptyset\right\}$$

where $E_A^L$ is the parametric domain of all active elements on hierarchical level $L$ and belongs to the parametric domain of active elements:

$$\boldsymbol{\Omega}_d = \bigcup_{L=0}^{P-1} E_A^L \quad \text{with} \quad E_A^L = \bigcup_e \boldsymbol{\Omega}_d^{e,L} \tag{60}$$

where $\boldsymbol{\Omega}_d^{e,L}$ represents the parametric domain of element $e$ on hierarchical level $L$. The parametric domains $\boldsymbol{\Omega}_d^{L+}$ and $\boldsymbol{\Omega}_d^{L-}$ are expressed as:

$$\boldsymbol{\Omega}_d^{L+} = \bigcup_{i=L+1}^{P-1} E_A^i \qquad \boldsymbol{\Omega}_d^{L-} = \bigcup_{i=0}^{L-1} E_A^i \tag{61}$$

As stated earlier, cf. eq. (56), the basis functions at level $L$ can be expressed as a linear combination of the bases at level $L+1$. When lower level bases are eliminated, the truncated hierarchical basis function space is obtained as:

$$\mathcal{A}_T = \bigcup_{L=0}^{P-1} \mathcal{A}_{T,a}^L \quad \text{with} \quad \mathcal{A}_{T,a}^L = \left\{ \tau_j^L \in \mathcal{A}_a^L : \ \sup \tau_i^L \nsubseteq E_A^{L+1} \right\} \tag{62}$$

where
$$\tau_i^L = \left\{ \tau_i^L \in \mathcal{N}^L : \ \tau_i^L = \sum S_{ij}^{L,L+1} N_j^{L+1} \right\} \tag{63}$$

Truncated hierarchical bases give a better conditioning of the system of equations and fulfill the partition of unity property [10, 11].

### 4.2. Multi-level implementation of hierarchical bases

Using Beziér extraction, the active elements are used in assembling the stiffness matrix for all levels which results in a global system of equations. In gradient elasticty for example, the resulting system of equations is:

$$\mathbf{K}\mathbf{b} = \mathbf{f} \tag{64}$$

where $\mathbf{K} = \mathbf{K}_1 + \mathbf{K}_2$, cf. eq. (34). $\mathbf{b}$ (which equals $\mathbf{a}$ for gradient elasticity) includes the degrees of freedom for control points from each hierarchical level and $\mathbf{K}$ is a sparse matrix with submatrices $\mathbf{K}^L$ corresponding to each hierarchical level $L$. Since only active elements are considered, $\mathbf{K}^L$ is very sparse.

12

It is noted that $\mathbf{K}$ does not incorporate the interaction between different hierarchical levels. This is incorporated through the hierarchical subdivision or refinement operator:

$$
\mathbf{M}_h = \begin{bmatrix}
\mathbf{I}^0 & \hat{\mathbf{M}}^{0,1} & \hat{\mathbf{M}}^{0,2} & \cdots & \hat{\mathbf{M}}^{0,P-1} \\
 & \mathbf{I}^1 & \hat{\mathbf{M}}^{1,2} & \cdots & \hat{\mathbf{M}}^{1,P-1} \\
 & & \mathbf{I}^2 & \cdots & \hat{\mathbf{M}}^{2,P-1} \\
 & & & \ddots & \\
\mathbf{0} & & & & \mathbf{I}^{P-1}
\end{bmatrix}
\tag{65}
$$

where

$$
I_{IJ}^L = \begin{cases} 1 & \text{for} \quad I = J \quad \text{and} \quad N_I^L \in \mathcal{A}_a^L \\ 0 & \text{else} \end{cases}
\tag{66}
$$

and the entries $\hat{\mathbf{M}}^{L,k}$ are defined as follows for truncated hierarchical basis functions:

$$
\hat{\mathbf{M}}^{L,k} = \begin{cases} S_{IJ}^{L,k} & \text{for} \quad N_I^L \in \mathcal{A}_+^L \quad \text{and} \quad N_J^K \in \mathcal{A}_-^L \\ 0 & \text{else} \end{cases}
\tag{67}
$$

in which $S_{IJ}^{L,k}$ is given in eq.(57). When the hierarchical subdivision operator $\mathbf{M}_h$ is used, the system of equations becomes:

$$
\mathbf{K}_h\,\mathbf{b}_h = \mathbf{f}_h \quad \text{where} \quad \mathbf{K}_h = \mathbf{M}_h\,\mathbf{KM}_h^T, \;\; \mathbf{f}_h = \mathbf{M}_h\,\mathbf{f}.
\tag{68}
$$

It is also noted that in a non-linear iteration procedure - e.g. in gradient plasticity, $\mathbf{K}$ is computed using $\mathbf{b}$ (and not $\mathbf{b}_h$) from the previous iteration. It is retrieved by using

$$
\mathbf{b} = \mathbf{M}_h^T \mathbf{b}_h.
\tag{69}
$$

## 5. Adaptive hierarchical refinement

To perform adaptive isogeometric analysis using NURBS, the following procedure is followed:

1. Solve the hierarchical system of equations $\mathbf{K}_h\mathbf{b}_h = \mathbf{f}_h$.
   - For gradient elasticity, $\mathbf{K}_h = f(\mathbf{K}_1, \mathbf{K}_2, \mathbf{M}_h)$, $\mathbf{b}_h = f(\mathbf{M}_h, \mathbf{a})$ and $\mathbf{f}_h = f(\mathbf{M}_h, \mathbf{f}^{ext})$

13

- For gradient plasticity, $\mathbf{K}_h = f(\mathbf{K}_{aa}, \mathbf{K}_{a\lambda}, \mathbf{K}_{\lambda a}, \mathbf{K}_{\lambda\lambda}, \mathbf{M}_h)$, $\mathbf{b}_h = f(\mathbf{M}_h, \mathrm{d}\mathbf{a}, \mathrm{d}\bar{\mathbf{\Lambda}})$ and $\mathbf{f}_h = f(\mathbf{M}_h, \mathbf{f}_e, \mathbf{f}_a, \mathbf{f}_\lambda)$

2. Project the solution on all active basis functions using $\mathbf{b} = \mathbf{M}_h^T \mathbf{b}_h$
3. Estimate the approximation error in each element

   - For gradient elasticity, the relative energy norm is used

   - For gradient plasticity, a measure of the plastic strain and the length scale are used

4. Mark elements to be refined according to step 3.
5. If some elements are marked for refinement,

   - Refine the elements

   - Transfer the state variables (gradient elasticity) and the history variables (gradient plasticity) from the old mesh to the new mesh

   - Return to step 1

6. If no elements are marked, stop the procedure

Clearly, the following are required: (I) marking of elements - mainly based on an error estimation technique; (II) a refinement strategy, and (III) data transfer between two consecutive levels/meshes.

*5.1. Element marking*

For gradient elasticity, the element error is estimated using the relative energy norm. The relative energy norm for each element, $e$, is calculated using the error in energy norm $\|e\|$ and the energy norm $\|U\|$ as follows [32]:

$$
\hat{\phi}_e = \frac{\|e\|_e}{\|U\|_e} = \frac{\sqrt{\frac{1}{2} \int_{\Omega_e} (\hat{\boldsymbol{\sigma}} - \boldsymbol{\sigma})^T \cdot (\mathbf{D}^e)^{-1} \cdot (\hat{\boldsymbol{\sigma}} - \boldsymbol{\sigma}) dS}}{\sqrt{\frac{1}{2} \int_{\Omega_e} \hat{\boldsymbol{\sigma}} \cdot (\mathbf{D}^e)^{-1} \cdot \hat{\boldsymbol{\sigma}} dS}} \tag{70}
$$

where $\hat{\boldsymbol{\sigma}}$ represents the analytical solution, $\boldsymbol{\sigma}$ represents the approximate solution and $\mathbf{D}^e$ is the material elastic stiffness matrix. Only two-dimensional plane-strain problems are considered in this work, so that:

$$
\mathbf{D}^e = \frac{E}{(1 + \nu)(1 - 2\nu)} \begin{bmatrix} 1 - \nu & \nu & 0 \\ \nu & 1 - \nu & 0 \\ 0 & 0 & \frac{1 - 2\nu}{2} \end{bmatrix} \tag{71}
$$

14

The exact solution is used when available, otherwise, a sufficiently finer mesh is used as reference. The element-wise errors ($\phi_Q$), where $Q$ is an element in mesh $\Omega$ with $N$ number of elements, are arranged in descending order – for $\Omega = \{Q_1, \cdots, Q_N\}$, $\phi_{Q_1} \geq \cdots \geq \phi_{Q_N}$. A marking parameter $\eta \in [0, 1]$ is defined such that $k$ elements are marked for refinement:

$$\mathcal{M} = Q_1, \cdots, Q_k \quad \text{with} \quad k = \text{ceil}(\eta N) \tag{72}$$

where the 'ceil()' function rounds up to the nearest integer. This approach is also referred to as the quantile marking strategy. It should be noted that when an element is already at the highest hierarchical level, it is *not* marked for refinement. Also, to ensure that the stiffness matrix $\mathbf{K}_h$ has a good condition number, elements adjacent to the marked elements are forced to be from the same level, or at most, two hierarchy levels [32].

According to Perić et al. [14], the relative energy norm can be used with classical elastoplasticity, as well as generalised plasticity models. Hence, we also adopt the error in energy norm with quantile marking for classical plasticity.

As stated earlier, for localisation problems using gradient plasticity, the length scale $\ell$ should be larger than the mesh size such that two to four elements lie within the localisation band [21, 22, 23]. If this is not the case, the model will not properly offer the needed regularisation. In the case of gradient plasticity, we use the following parameter:

$$d = \frac{h_e}{\ell} \tag{73}$$

where $h_e$ is the size of element $e$. The lower the value of $d$, the more capable the mesh is to capture a localisation band.

*5.2. Refinement strategy*

Hierarchical refinement is performed based on the concept of active and inactive elements. Thus, all elements in different hierarchy levels exist *a priori* before computation, but, the relevant elements to be activated are chosen successively such that at each instant, the whole geometry is fully covered. To this end, two indicator arrays, each of the same size as the number of elements, are defined and initialised as **false**:

- $\mathbf{E}_a$ - indicator of active elements. $E_a^i$ is true when element $i$ is active

15

- $\mathbf{E}_{ac}$ - indicator of active child elements. $E_{ac}^i$ is true when the child elements of element $i$ are active

Based on these two arrays, the indicators for the total number of basis functions across all levels are defined. The basis functions are defined as $\mathbf{N} = \{N^i\}$, $i = 1, 2, \cdots, n_b$ where $n_b$ is the total number of basis functions. The following Boolean arrays are defined and initialised as **false**, see section 4:

- $\mathbf{A}_a$ - indicator of basis function in the hierarchical basis function space $\mathcal{A}$ or $\mathcal{A}_T$, cf. eq. (58) and eq. (62). $A_a^i$ is true when $N^i \in \mathcal{A}$ or $\mathcal{A}_T$

- $\mathbf{A}_-$ - indicator of basis function in the hierarchical basis function space $\mathcal{A}_-$, cf. eq. (59). $A_-^i$ is true when $N^i \in \mathcal{A}-$

- $\mathbf{A}_+$ - indicator of basis function in the hierarchical basis function space $\mathcal{A}_+$, cf. eq. (59). $A_+^i$ is true when $N^i \in \mathcal{A}+$

Let some elements $E_r$ be elements marked for refinement and $E_{rc}$ be all child elements of $E_r$. To obtain the new list of active elements and active child elements, the following procedure is followed:

- Obtain the old list of $\mathbf{E}_a$ and $\mathbf{E}_{ac}$

- Set $\mathbf{E}_a(E_r) = \textbf{false}$ and $\mathbf{E}_{ac}(E_r) = \textbf{true}$

- Set $\mathbf{E}_a(E_{rc}) = \textbf{true}$ and $\mathbf{E}_{ac}(E_{rc}) = \textbf{false}$

*5.3. Transfer of state vector and history variables*

When moving from a time step $t$ to time step $t + \Delta t$ where some elements have been marked for refinement, the old state vector $^t\mathbf{b}$ needs to be mapped onto the new state $^{t+\Delta t}\mathbf{b}$. We call this mapping transfer operation $\mathcal{T}^0$. This is done in a straightforward manner, as follows:

$$^{t+\Delta t}\mathbf{b}^{L+1} = (\tilde{\mathbf{S}}^{L,L+1})^T \, ^t\mathbf{b}^L \tag{74}$$

in which $L$ is the hierarchical level and $\tilde{\mathbf{S}}^{L,L+1}$ is the modified refinement operator:

$$\tilde{S}_{IJ}^{L,L+1} = \begin{cases} S_{IJ}^{L,L+1} & \text{for} \quad N_J^{L+1} \in \, ^{t+\Delta t}\mathcal{A}^{L+1} \text{ or } ^{t+\Delta t}\mathcal{A}_T^{L+1} \\ 0 & \text{else} \end{cases} \tag{75}$$

16

where $^{t+\Delta t}\mathcal{A}^{L+1}$ and $^{t+\Delta t}\mathcal{A}_T^{L+1}$ are hierarchical basis function spaces at hierarchical level $L+1$ and time step $t+\Delta t$. The transfer of the state vector from the old control points to the new control points suffices for gradient elasticity.

In the case of gradient plasticity, there are also history variables at the old integration points which need to be transferred to the integration points of the new mesh. This is done in three mapping steps:

1. $\mathcal{T}^1$ - the history variables from the old integration points are extrapolated to the control points of the old mesh;
2. $\mathcal{T}^2$ - these control variables on the old mesh are mapped to the control points of the new mesh, and
3. $\mathcal{T}^3$ - the history data is interpolated from the control points of the new mesh to the integration points of the new mesh

To perform $\mathcal{T}^1$, a global least-squares projection is used [21]. For any history variable, the control variables contained in a vector $\boldsymbol{\zeta}^c$ can be obtained from the values at the Gauss points contained in a vector $\boldsymbol{\zeta}^g$ by solving [33]:

$$\mathbf{M}\boldsymbol{\zeta}^c = \int_V \mathbf{h}^T \boldsymbol{\zeta}^g \mathrm{d}V \tag{76}$$

where $\mathbf{M}$ is the least-squares fit matrix or Gramm matrix given by:

$$\mathbf{M} = \int_V \mathbf{h}\mathbf{h}^T \mathrm{d}V \tag{77}$$

and $\mathbf{h}$ a vector that contains the NURBS shape functions used to discretise the relevant history variable (e.g. the plastic multiplier as in eq. (41)). $\mathcal{T}^2$ is done in a similar way as $\mathcal{T}^0$ for the state vector. $\mathcal{T}^3$ is performed by interpolation using the shape functions:

$$\boldsymbol{\zeta}^g = \mathbf{h}\boldsymbol{\zeta}^c. \tag{78}$$

It is noted that we transfer both the old history variables (at the previous, converged loadstep) and the current history variables. The mapping procedure is a shape function transfer. In the extrapolation operation $\mathcal{T}^1$, a global least-squares projection has been used. Other possibilities include the use of the superconvergent patch recovery technique and the use of local least-squares projection [13, 17]. While these alternatives reduce the computational

cost, the global least squares projection remains the most accurate [17]. Instead of a shape function transfer, the closest point transfer can also be used. In this method, the history variable in the new integration point is computed from the integration point that is spatially closest to it in the old mesh [17].

## 6. Numerical examples

We consider three classes of problems: gradient elasticity, classical plasticity and gradient plasticity. A plane strain assumption is made in all cases.

### 6.1. Gradient elasticity

Two problems are addressed - a thick cylinder subjected to external pressure for which an exact solution exists, and an L-shaped beam subjected to tractions. In both problems, Young's modulus $E = 8100$ MPa, Poisson ratio $\nu = 0.35$ and the length scale $\ell = 0.01$ m. Meshes with 5 hierarchical levels have been used. At each level $k$ $(k = 1, \cdots, 5)$, $2^k \times 2^k$ elements are employed to discretise the domain.

#### 6.1.1. Thick hollow cylinder subjected to external pressure
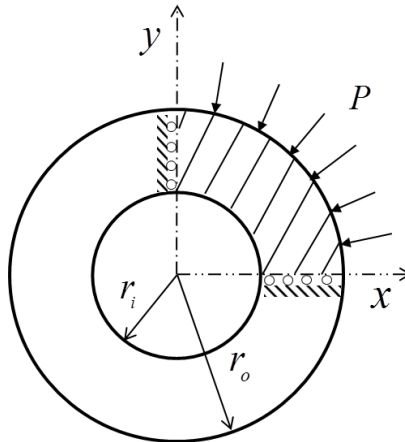


Figure 1: Geometry and dimensions of cylinder subjected to external pressure

The cylinder considered has an internal radius, $r_i = 0.05$ m and an external radius, $r_o = 0.5$ m. It is subjected to an external pressure $P = 1$ MPa. Only a quarter of the cylinder is considered due to symmetry, see figure 1. The exact solution is given in [34]. The error in energy norm is used to mark
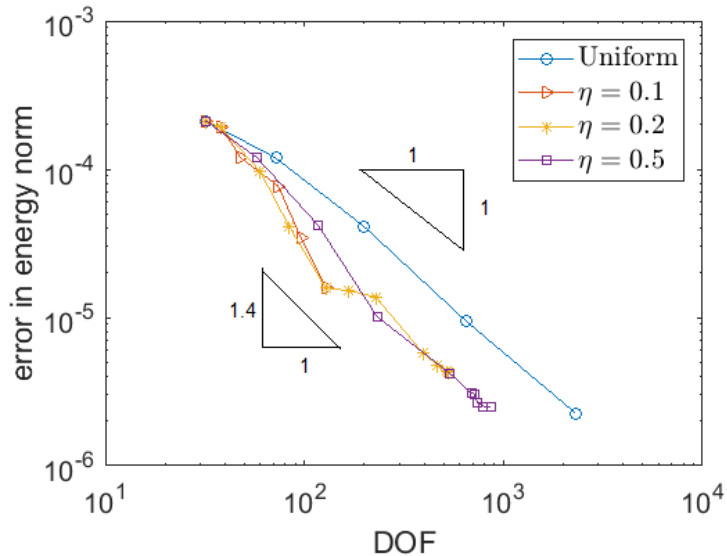
Figure 2: Convergence rates for different values of $\eta$. The results of hierarchical refinement and uniform refinement are shown.

elements for refinement using quantile marking. Three values of $\eta$ are used - $\eta = \{0.1, 0.2, 0.5\}$. Uniform mesh refinement to the highest hierarchy level is also considered.

It is necessary to impose higher-order boundary conditions on the cylinder [34]. The set of control points immediately next to the boundaries are used as follows [4]:

$$
\begin{aligned}
\frac{\partial u_y}{\partial x} &= 0; \quad \text{enforced as} \quad u_y(2, j) = u_y(1, j) \quad \text{at the left boundary} \\
\frac{\partial u_x}{\partial y} &= 0; \quad \text{enforced as} \quad u_x(i, 2) = u_x(i, 1) \quad \text{at the bottom boundary}
\end{aligned}
\tag{79}
$$

The boundary conditions have been imposed on control points across all hierarchy levels *a priori*.

The convergence rates are illustrated in figure 2. For uniform refinement, a convergence rate of $-P/2 = -1$ is obtained. It is clear that with hierarchical refinement, there is a reduction in the error with an improved rate of convergence. Hence, with less degrees of freedom, a higher accuracy, and therefore, a higher efficiency is obtained which is the main goal of adaptive analysis. The value of $\eta$ does not seem to have a significant influence on the

19

results. For different values of $\eta$, the elements that are refined also differ (figure 3). However, the same trend is observed for the refinement toward the inner circle and hence the convergence rate hardly changes.

The $\sigma_{xy}$ plots and the relative error $\phi_e$ (cf. eq. (70)) in each element are shown in figures 3 and 4 respectively. The fact that there is no refinement close to the left and bottom boundaries is an indication that the boundary conditions have been imposed consistently. The error is concentrated at the inner boundary where the gradient of the strain is high. This is in line with results obtained in [4].



(a) $\sigma_{xy}$, $\eta = 0.1$

(b) $\sigma_{xy}$, $\eta = 0.2$

(c) $\sigma_{xy}$, $\eta = 0.5$

(d) $\sigma_{xy}$, uniform
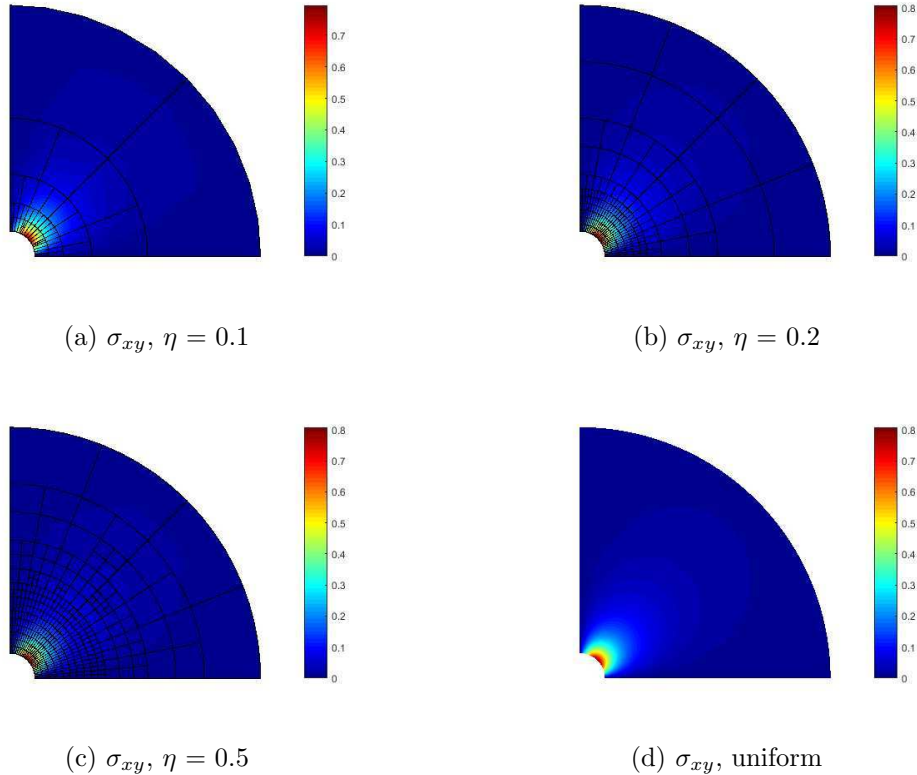
Figure 3: $\sigma_{xy}$ [MPa] components of the stress of each element for different values of $\eta$.

*6.1.2. L-shaped panel subjected to traction*

An L-shaped panel with dimension $a = 30$ m and subjected to a traction $t = 1$ MPa is considered next, figure 5. The top boundary is restricted in

(a) $\phi_e$, $\eta = 0.1$

(b) $\phi_e$, $\eta = 0.2$

(c) $\phi_e$, $\eta = 0.5$
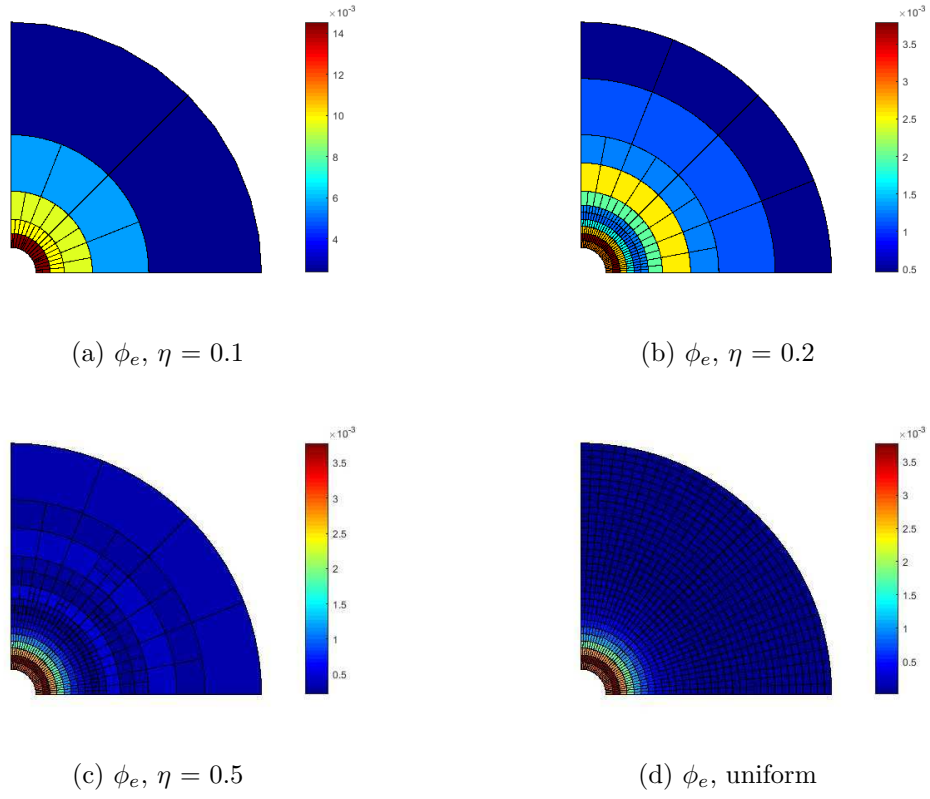
(d) $\phi_e$, uniform

Figure 4: Relative error norm $\hat{\phi}_e$ of each element for different values of $\eta$.
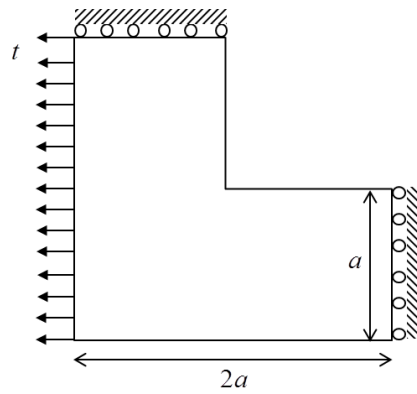


Figure 5: Geometry of L-shaped panel
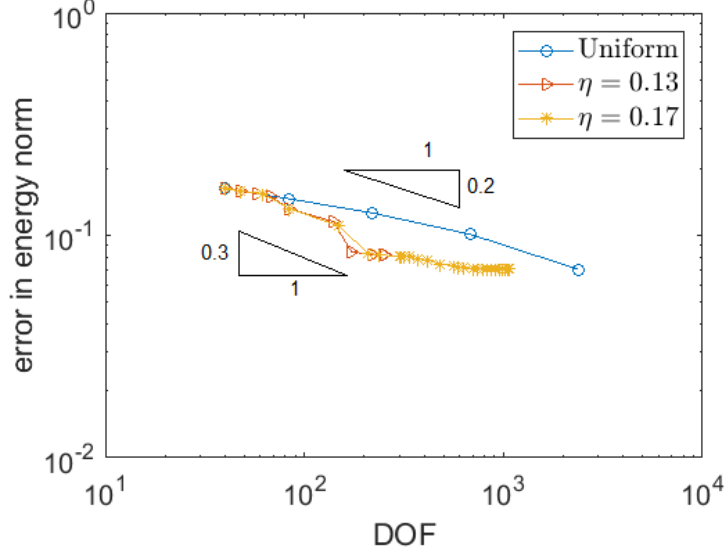
Figure 6: Indicative convergence for uniform and hierarchical refinement for L-shaped panel.

the vertical direction and the right boundary is constrained in the horizontal direction. To estimate the error, we use results of a mesh with $2^6 \times 2^6$ elements as the reference solution. Since the error estimation is now element-based, we use a slightly modified relation to calculate the relative error in each element [5]:

$$
\hat{\phi}_e = \frac{\phi_e}{\sqrt{\frac{1}{2}\sum_{i=1}^4 \hat{\boldsymbol{\sigma}}_i \cdot (\mathbf{D}^e)^{-1} \cdot \hat{\boldsymbol{\sigma}}_i}} = \frac{\sqrt{\frac{1}{2}\sum_{i=1}^4 (\hat{\boldsymbol{\sigma}} - \boldsymbol{\sigma})_i^T \cdot (\mathbf{D}^e)^{-1} \cdot (\hat{\boldsymbol{\sigma}} - \boldsymbol{\sigma})_i}}{\sqrt{\frac{1}{2}\sum_{i=1}^4 \hat{\boldsymbol{\sigma}}_i \cdot (\mathbf{D}^e)^{-1} \cdot \hat{\boldsymbol{\sigma}}_i}}
$$

(80)

where summation is over the vertices; $\hat{\boldsymbol{\sigma}}_i$ and $\boldsymbol{\sigma}_i$ denote the stress at the vertex $i$ for the reference solution and the numerical solution respectively.

The convergence plot is given in figure 6 but only serves as an indicator considering the reference solution employed. It again shows that hierarchical refinement reduces the error while improving the rate of convergence. Quantile marking for element refinement is considered here with $\eta$ values of 0.13 and 0.17. The $\sigma_{xy}$ stress component as well as the relative error in each element are presented in figure 7 up to results for the highest hierarchical

22

level.

It is clear from figures 7 and 8 that the refinement tends towards the inner corner where there is a stress concentration. The gradient elasticity effect in removing the stress singularity is also seen near the singularity. It is emphasised that the plots are indicative considering the reference solution adopted, and hence, the expected convergence rate is not retrieved as in the previous example. However, an improved rate of convergence is obtained compared to that of uniform refinement, see Figure 6.

In figure 9, different length scales have been considered for $\eta = 0.17$. For a higher length scale, the regularisation of the stress singularity becomes more pronounced and the error level reduces.

## 6.2. Classical plasticity

In a step-wise manner, classical plasticity is considered as the first non-linear problem. We again consider a plane strain cylinder (a quarter of the geometry due to symmetry) but this time subjected to internal pressure $P_i$. The cylinder, with inner radius $a$ and outer radius $b$, is assumed to be elastic-perfectly plastic using the Von Mises yield criterion. Beyond a certain critical pressure $P_{cr}$, there is a region of plastic deformation, $a \leq r \leq c$, defined by the radius $r$ and the elastic-plastic boundary $c$. The value of $c$ is determined by solving the following equation numerically [35, 36]:

$$P_i = k\left(1 - \frac{c^2}{b^2} + \ln\frac{c^2}{a^2}\right) \tag{81}$$

where $k = \sigma_y/\sqrt{3}$ and $\sigma_y$ is the yield stress. The critical pressure is calculated using:

$$P_{cr} = \frac{k\left(1 - a^2/b^2\right)}{\sqrt{1 + \frac{1}{3}(1 - 2\nu)^2\left(\frac{a^4}{b^4}\right)}} \tag{82}$$

For a cylinder with $a = 0.1$ m, $b = 0.2$ m, $\nu = 0.3$, $\sigma_y = 0.24$ GPa and $E = 210$ GPa, $P_{cr} = 0.10375$ GPa. For an applied pressure of 0.18 GPa($> P_{cr}$), $c = 0.15979$ m. In the plastic region, the stresses are ($\sigma_{r\theta} = 0$):

$$\sigma_r = -k\left(1 - \frac{c^2}{b^2} + \ln\frac{c^2}{r^2}\right), \quad \sigma_\theta = k\left(1 + \frac{c^2}{b^2} - \ln\frac{c^2}{r^2}\right); \quad \text{for } a < r < c \tag{83}$$

23
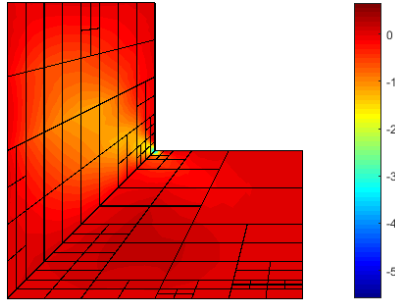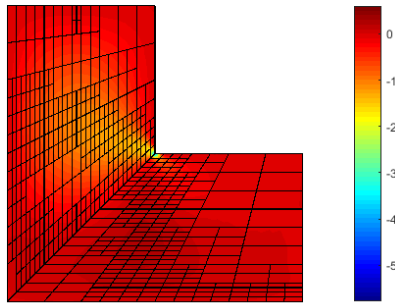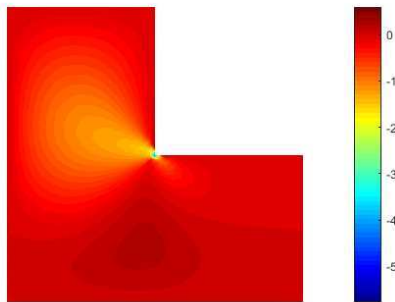
(a) $\eta = 0.13$



(b) $\eta = 0.17$



(c) uniform

Figure 7: $\sigma_{xy}$ [MPa] components of the stress for different values of $\eta$.

24
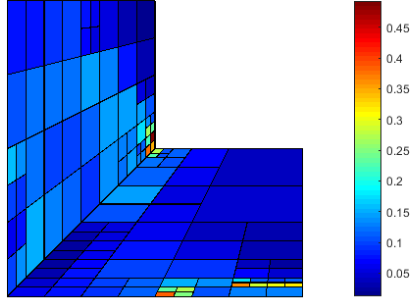
(a) $\eta = 0.13$
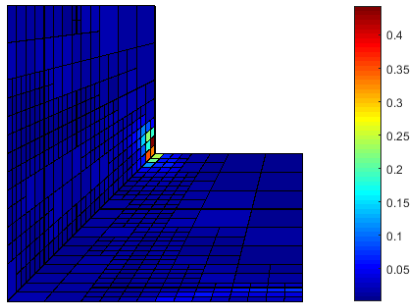


(b) $\eta = 0.17$
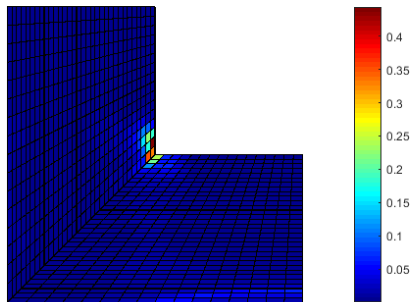


(c) uniform

Figure 8: Relative error norm $\hat{\phi}_e$ of elements for different values of $\eta$.
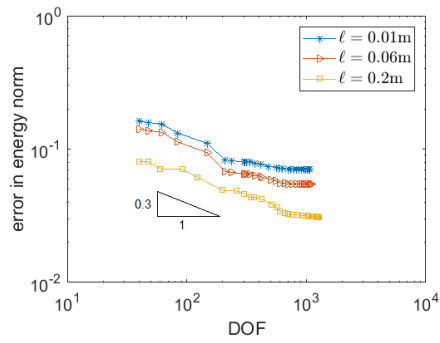
(a) convergence plot
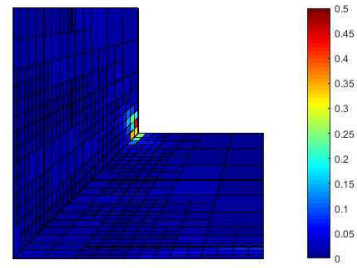
(b) $\ell = 0.01$ m
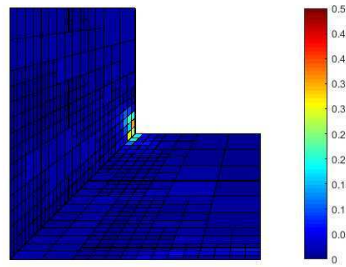
(c) $\ell = 0.06$ m
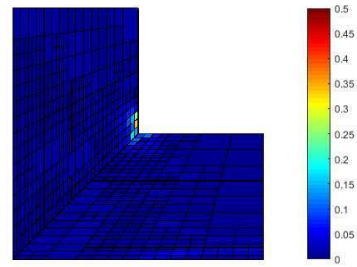
(d) $\ell = 0.2$ m

Figure 9: Convergence plot and error norm of elements $\hat{\phi}_e$ for different values of the length scale $\ell$; $\eta = 0.17$

.

(a) plastic strain



(b) error in energy norm



(c) $\sigma_{xy}$



(d) $\sigma_{xy}$ uniform
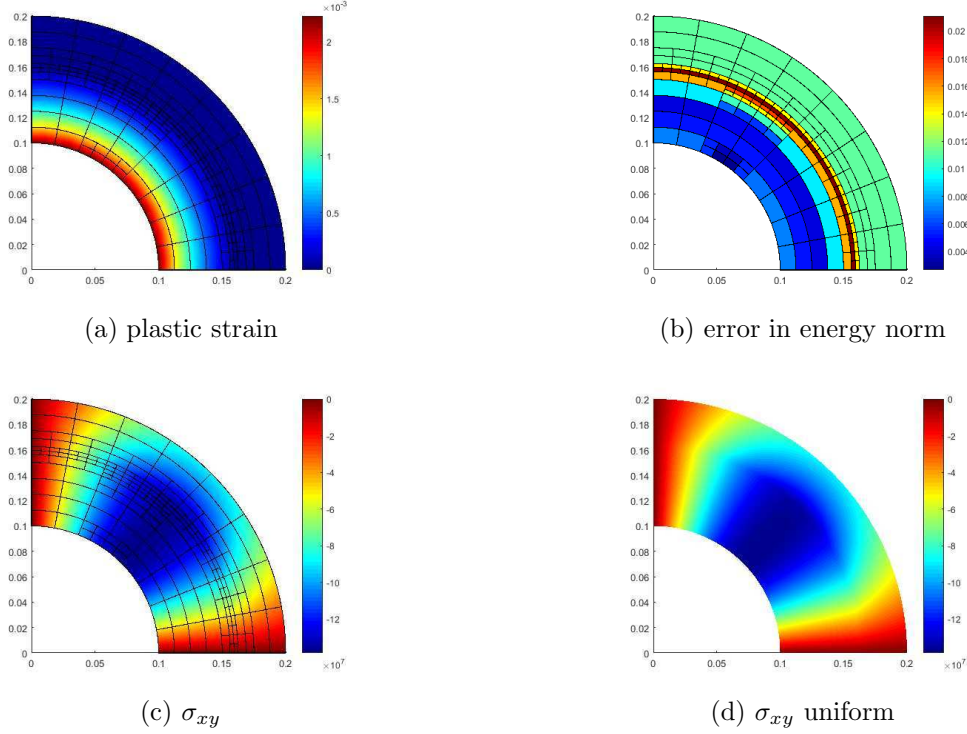
Figure 10: Plastic strain, error in energy norm, $\sigma_{xy}$ [MPa] as well as its analytical solution for elastic-perfectly plastic cylinder.

In the elastic region, they are computed as

$$\sigma_r = -k\left(1 - \frac{c^2}{b^2} + \ln\frac{c^2}{r^2}\right), \quad \sigma_\theta = k\left(1 + \frac{c^2}{b^2} - \ln\frac{c^2}{r^2}\right); \quad \text{for } c < r < b \quad (84)$$

The problem is solved using adaptive isogeometric analysis. Similar to gradient elasticity, the relative error in energy norm is adopted with quantile marking using $\eta = 0.2$. As alluded to before, the relative energy norm can be used for classical plasticity and for plasticity models in generalised continua [14]. Classical plasticity has been used here to validate that the transfer of the variables is consistent, and for this purpose, this marking strategy suffices. The plots of the plastic strain and the $\sigma_{xy}$ component of the stress are presented in figure 10. $\sigma_{xy}$ is retrieved as $\sigma_{xy} = (\sigma_r - \sigma_\theta)(xy/r^2)$. A good match with the reference result is obtained, which indicates that the hierarchical refinement model works well and that the variables are transferred properly.

Moreover, from the plot of the plastic strain in figure 10a, the radius $c$ at the elastic-plastic boundary is close to the analytical value of 0.16. The relative error in energy norm is also plotted and it is clear that the error is highest at the elastic-plastic boundary.

*6.3. Gradient plasticity*
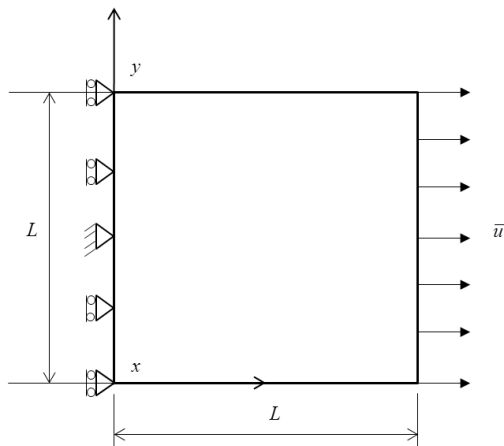


Figure 11: Geometry of square plate under uniaxial tension.

Finally, a localisation problem is considered using implicit gradient plasticity [31]. The problem is illustrated in figure 11. A square panel of length $L$ = 10 m is constrained on the left side and uniaxial tension is applied on the opposite side. For the material parameters, $E = 20000$ N/mm$^2$, H = 2000 N/mm$^2$, $\sigma_{y,0} = 2$ N/mm$^2$, $\beta = 3500$ and $\ell = 0.7$ mm. A mesh with four levels is considered. At each level $k$ ($k = 1, \cdots, 4$), $2^{k+1} \times 2^{k+1}$ elements are employed to discretise the domain. To trigger localisation, the bottom left element in the coarsest mesh and all children down the hierarchy are weakened by assuming a 5% reduction in the yield strength.

Elements are marked for refinement only after the nonlocal plastic strain has become non-zero. Let $\kappa_{max}$ be the maximum plastic strain. Elements with up to 9% of $\kappa_{max}$ are marked for refinement and refinement is continued until $d < 0.5$ (cf. (73)). Hence, there is progressive refinement as the deformation localises. This is clear from the results which are shown in figure 12. The adopted marking strategy enables element refinement only after the onset of localisation and sets the highest refinement level based on the value of length scale.
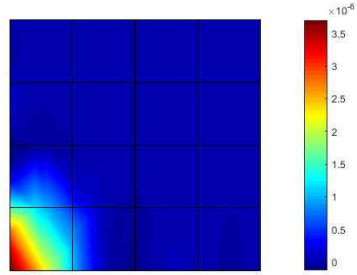
(a) $\bar{u} = 0.00091$ mm
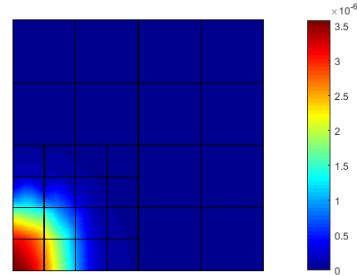
(b) $\bar{u} = 0.00091$ mm
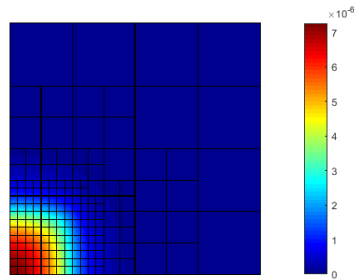
(c) $\bar{u} = 0.00093$ mm
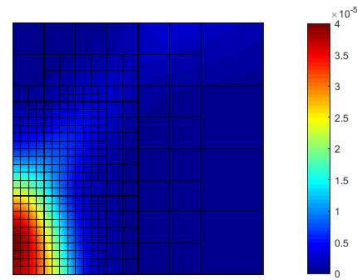
(d) $\bar{u} = 0.00100$ mm
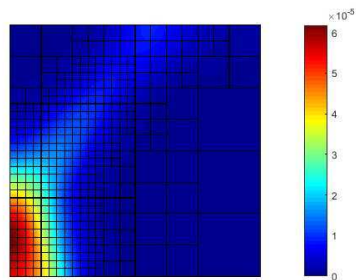
(e) $\bar{u} = 0.00101$ mm
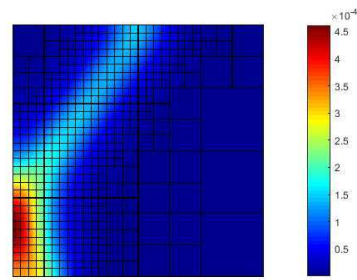
(f) $\bar{u} = 0.00114$ mm

Figure 12: Nonlocal effective plastic strain: Adaptive refinement as localisation band progresses.

Here, the robustness of the scheme is also apparent since we start with elements that would normally not allow the shearband to develop. This is particularly seen in the first case (in figure 12) when localisation starts. With further refinement, the band propagates smoothly. It is important to ensure that the presented results are similar to those obtained from a standard uniformly refined mesh in the literature [31, 20]. A comparison is shown for the local and nonlocal effective plastic strain (figure 13). Further confirmation



(a) local, hierarchical



(b) local, uniform



(c) nonolocal, hierarchical



(d) nonolocal, uniform
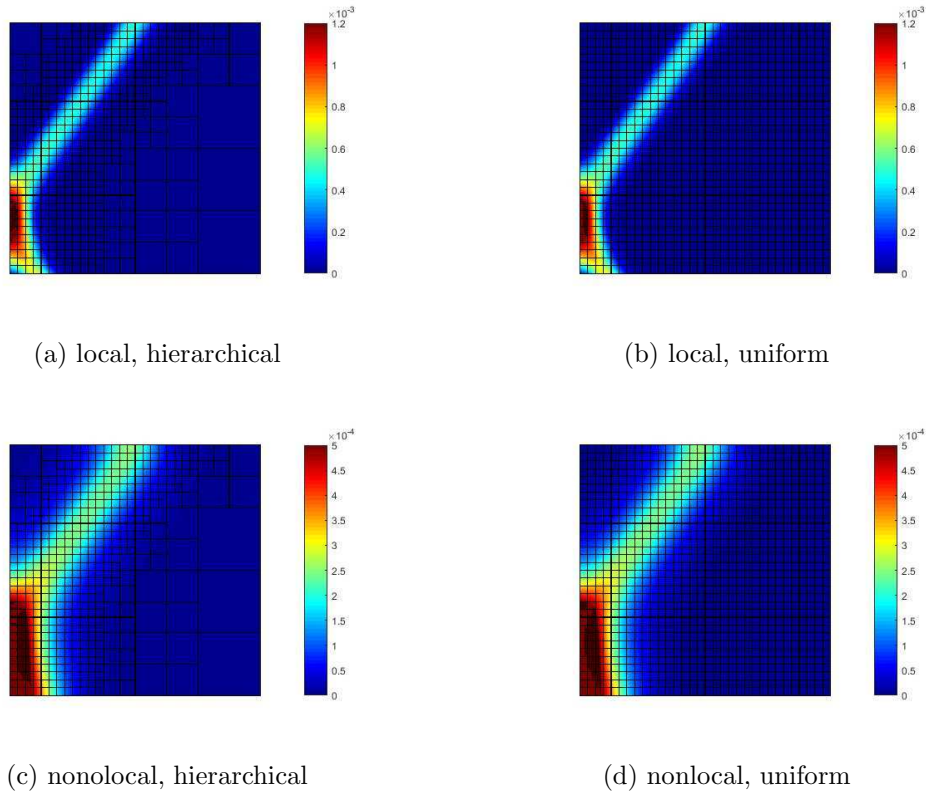
Figure 13: Comparison of local and nonlocal effective plastic strains for standard and adaptive implicit gradient plasticity, $\bar{u} = 0.0012$ mm. The local measure has a less pronounced nonlocal or smearing effect.

is pursued by comparing the force-displacement curves which show also very good agreement, see figure 14.
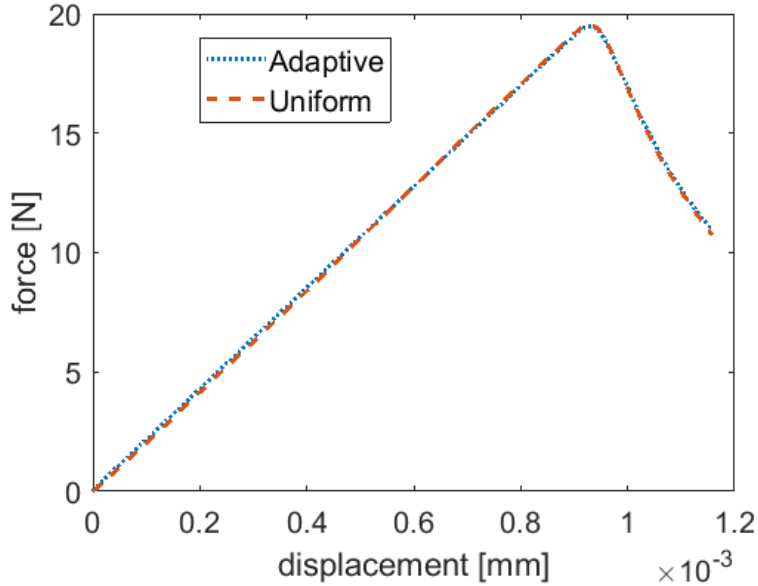
Figure 14: Force-displacement curves for uniform and adaptive implicit gradient plasticity analyses.

## 7. Conclusion

This work has extended adaptive isogeometric analysis to strain-gradient continuum models - gradient elasticity and gradient plasticity. Hierarchical refinement using truncated multi-level basis functions which interact through a subdivision operator has been adopted within the Beziér element framework. Elements are marked for refinement using the relative error in energy norm for gradient elasticity. For gradient plasticity, a measure of the effective plastic strain is used to mark and refine elements which need to better capture the localising deformation. Refinement is based on the concept of elements and their child elements which are activated or deactivated accordingly. When an element is refined, the current as well as the old history variables are transferred from the integration points of the old mesh to its control points using global least-squares approximation. Next, they are transferred to the control points of the new mesh using a modified subdivision operator. They are finally transferred to the integration points of the new mesh by shape function interpolation. The results have been verified against benchmarks in the literature. A robust computational framework for engi-

31

neering analysis has been developed combining the flexibility, exact geometry representation, and expedited design-through-analysis of isogeometric analysis, size-effect incorporation and mesh-objective results of gradient-enhanced continua, the standard convenient data structure of finite element analysis and the improved efficiency of adaptive hierarchical refinement.

## References

[1] T. J. Hughes, J. A. Cottrell, Y. Bazilevs, Isogeometric analysis: CAD, finite elements, NURBS, exact geometry and mesh refinement, Computer Methods in Applied Mechanics and Engineering 194 (2005) 4135–4195.

[2] C. V. Verhoosel, M. A. Scott, T. J. Hughes, R. de Borst, An isogeometric analysis approach to gradient damage models, International Journal for Numerical Methods in Engineering 86 (2011) 115–134.

[3] M. Kästner, P. Metsch, R. de Borst, Isogeometric analysis of the Cahn–Hilliard equation–a convergence study, Journal of Computational Physics 305 (2016) 360–371.

[4] P. Fischer, M. Klassen, J. Mergheim, P. Steinmann, R. Müller, Isogeometric analysis of 2D gradient elasticity, Computational Mechanics 47 (2011) 325–334.

[5] I. Kolo, H. Askes, R. de Borst, Convergence analysis of Laplacian-based gradient elasticity in an isogeometric framework, Finite Elements in Analysis and Design 135 (2017) 56–67.

[6] H. Askes, E. C. Aifantis, Gradient elasticity in statics and dynamics: An overview of formulations, length scale identification procedures, finite element implementations and new results, International Journal of Solids and Structures 48 (2011) 1962–1990.

[7] R. de Borst, L. J. Sluys, H.-B. Mühlhaus, J. Pamin, Fundamental issues in finite element analyses of localization of deformation, Engineering Computations 10 (1993) 99–121.

[8] O. C. Zienkiewicz, J. Z. Zhu, A simple error estimator and adaptive procedure for practical engineerng analysis, International Journal for Numerical Methods in Engineering 24 (1987) 337–357.

[9] C. Giannelli, B. Jüttler, H. Speleers, THB-splines: The truncated basis for hierarchical splines, Computer Aided Geometric Design 29 (2012) 485–498.

[10] P. Hennig, S. Müller, M. Kästner, Bézier extraction and adaptive refinement of truncated hierarchical NURBS, Computer Methods in Applied Mechanics and Engineering 305 (2016) 316–339.

[11] L. Chen, E. J. Lingen, R. de Borst, Adaptive hierarchical refinement of NURBS in cohesive fracture analysis, International Journal for Numerical Methods in Engineering 112 (2017) 2151–2173.

[12] M. Ortiz, J. Quigley IV, Adaptive mesh refinement in strain localization problems, Computer Methods in Applied Mechanics and Engineering 90 (1991) 781–804.

[13] A. Khoei, S. Gharehbaghi, A. Tabarraie, A. Riahi, Error estimation, adaptivity and data transfer in enriched plasticity continua to analysis of shear band localization, Applied Mathematical Modelling 31 (2007) 983–1000.

[14] D. Perić, J. Yu, D. Owen, On error estimates and adaptivity in elasto-plastic solids: Applications to the numerical simulation of strain localization in classical and Cosserat continua, International Journal for Numerical Methods in Engineering 37 (1994) 1351–1379.

[15] H. Javani, R. Peerlings, M. Geers, Consistent remeshing and transfer for a three dimensional enriched mixed formulation of plasticity and non-local damage, Computational Mechanics 53 (2014) 625–639.

[16] X. Ju, R. Mahnken, Goal-oriented adaptivity for linear elastic micro-morphic continua based on primal and adjoint consistency analysis, International Journal for Numerical Methods in Engineering 112 (2017) 1017–1039.

[17] P. Hennig, M. Ambati, L. De Lorenzis, M. Kästner, Projection and transfer operators in adaptive isogeometric analysis with hierarchical B-splines, Computer Methods in Applied Mechanics and Engineering 334 (2018) 313–336.

[18] E. C. Aifantis, On the role of gradients in the localization of deformation and fracture, International Journal of Engineering Science 30 (1992) 1279–1299.

[19] B. Altan, E. Aifantis, On some aspects in the special theory of gradient elasticity, Journal of the Mechanical Behavior of Materials 8 (1997) 231–282.

[20] R. A. B. Engelen, M. G. D. Geers, F. P. T. Baaijens, Nonlocal implicit gradient-enhanced elasto-plasticity for the modelling of softening behaviour, International Journal of Plasticity 19 (2003) 403–433.

[21] I. Kolo, R. de Borst, An isogeometric analysis approach to gradient-dependent plasticity, International Journal for Numerical Methods in Engineering 113 (2018) 296–310.

[22] G. Pijaudier-Cabot, A. Huerta, Finite element analysis of bifurcation in nonlocal strain softening solids, Computer Methods in Applied Mechanics and Engineering 90 (1991) 905–919.

[23] R. de Borst, H.-B. Mühlhaus, Gradient-dependent plasticity: Formulation and algorithmic aspects, International Journal for Numerical Methods in Engineering 35 (1992) 521–539.

[24] H. Askes, J. Pamin, R. de Borst, Dispersion analysis and element-free Galerkin solutions of second-and fourth-order gradient-enhanced damage models, International Journal for Numerical Methods in Engineering 49 (2000) 811–832.

[25] L. H. Poh, S. Swaddiwudhipong, Gradient-enhanced softening material models, International Journal of Plasticity 25 (2009) 2094–2121.

[26] M. G. Cox, The numerical evaluation of B-splines, IMA Journal of Applied Mathematics 10 (1972) 134–149.

[27] C. de Boor, On calculating with B-splines, Journal of Approximation Theory 6 (1972) 50–62.

[28] M. J. Borden, M. A. Scott, J. A. Evans, T. J. Hughes, Isogeometric finite element data structures based on Bézier extraction of NURBS, International Journal for Numerical Methods in Engineering 87 (2011) 15–47.

[29] R. de Borst, L. Chen, The role of Bézier extraction in adaptive isogeometric analysis: Local refinement and hierarchical refinement, International journal for numerical methods in engineering 113 (2018) 999–1019.

[30] J. Y. Shu, W. E. King, N. A. Fleck, Finite elements for materials with strain gradient effects, International Journal for Numerical Methods in Engineering 44 (1999) 373–391.

[31] I. Kolo, R. de Borst, Dispersion and isogeometric analyses of second-order and fourth-order implicit gradient-enhanced plasticity models, International Journal for Numerical Methods in Engineering 114 (2018) 431–453.

[32] L. Chen, R. de Borst, Adaptive refinement of hierarchical T-splines, Computer Methods in Applied Mechanics and Engineering 337 (2018) 220–245.

[33] T. J. Mitchell, S. Govindjee, R. L. Taylor, A method for enforcement of Dirichlet boundary conditions in isogeometric analysis, in: Recent Developments and Innovative Applications in Computational Mechanics, Springer, 2011, pp. 283–293.

[34] A. Zervos, S.-A. Papanicolopulos, I. Vardoulakis, Two finite-element discretizations for gradient elasticity, Journal of Engineering Mechanics 135 (2009) 203–213.

[35] J. Lubliner, Plasticity Theory, Dover Publications, Inc., Mineola, New York, 2008.

[36] E. A. de Souza Neto, D. Peric, D. R. Owen, Computational Methods for Plasticity: Theory and Applications, John Wiley & Sons, Chichester, 2011.